IEEE/ASME TRANSACTIONS ON
MECHATRONICS

IEEE Xplore® Digital Library
http://ieeexplore.ieee.org/Xplore

Field Sensor Bias Calibration with Angular-Rate Sensors: Theory and Experimental Evaluation with Application to Magnetometer Calibration

Giancarlo Troni, *Member, IEEE,* Louis L. Whitcomb, *Fellow, IEEE*

***Abstract*—Field sensors, such as magnetometers and accelerometers, are widely used sensors for attitude estimation, yet their accuracy is limited by sensor measurement bias. This paper reports a novel methodology for estimating the sensor bias of three-axis field sensors. Our approach employs three-axis angular velocity measurements from an angular-rate gyroscope to estimate the three-axis field sensor measurement bias that, when properly calibrated, can significantly improve attitude estimation. We report three methods implementing this approach based on batch linear least squares, real time Kalman filter, and real time adaptive identification. Assuming the field is constant, our methods impose less restrictive conditions for the movements of the instrument required for calibration than previously reported methods, do not require a priori knowledge of the field (e.g. the magnitude of the local magnetic field) or the attitude of the instrument, and also ensure convergence for the estimated parameters. The proposed methods are evaluated and compared with the previously reported methods with numerical simulation and in a comparative laboratory and field experimental evaluation with the sensors onboard an underwater robot vehicle. Finally, as an application example of the magnetometer bias calibration, the proposed methods are used to improve the estimation of the position of an underwater vehicle in Monterey Bay at 2,800 m depth.**

***Index Terms*—Calibration and identification, estimation, adaptive control, Kalman filter, sensor fusion, robotics, field sensors, magnetometers, navigation, underwater vehicles, Doppler navigation.**

I. Introduction

Field sensors, such as magnetometers and accelerometers, measure the strength and the direction of a field in the instrument frame and are widely used in many applications. This kind of sensors are commonly used to estimate the attitude of the system—for example in vehicle navigation systems (e.g., space, air, ground, and marine vehicles) where it is critical to estimate the attitude of the system for accurate performance. Field sensors such as magnetometers and accelerometers are also commonly used in personal electronics devices for example for augmented reality applications, or providing to the user navigation directions. Magnetometers can measure Earth's local magnetic field vector and thus determine the device heading, Figure 1(a). Accelerometers can measure in the absence of accelerations the device's inclination with respect to the Earth's local gravity vector and thus determine the local horizontal plane and vertical direction—i.e. roll and pitch, Figure 1(b). Currently many integrated devices incorporate angular-rate gyroscopes—that measure the angular rotation rate of the device—together with accelerometers and magnetometers to enable dynamic estimation of the full attitude (e.g., heading, pitch and roll) of the instrument. Several methods are available to estimate the attitude with these sensors—the reader is directed to Crassidis et al. for a review of attitude estimation methods [1].

All of these sensors are affected by biases, scale factors, and non-orthogonality of their measurements. Sensor calibration is critical for accurate performance, specially for attitude estimation with these devices. A common and relevant calibration problem that affects field sensors is a measurement bias. The methods reported herein are useful in the scenario in which field sensor (such as a magnetometer or accelerometer) must be calibrated for field sensor bias. For example, magnetometers are highly affected by magnetic field biases that can cause erroneous measurements that can change over time (i.e. whenever the vehicle is reconfigured to accommodate new instruments or payloads). Accelerometers also have to be calibrated to estimate sensor measurement bias that can vary with time and with instrument temperature. For applications in which continuous calibration is required for accurate performance, real time, adaptive sensor bias estimation is desirable.

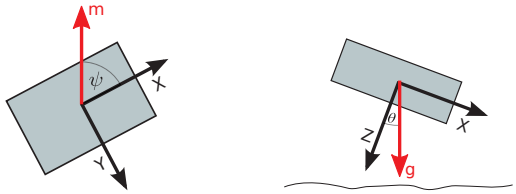

(a) Magnetometers (b) Accelerometers

Fig. 1. Examples of field sensors: (a) Magnetometers measure the local magnetic field. (b) Accelerometers at rest measure the local gravitational field.

This paper reports a novel general approach to calibrate field sensors based on angular rate sensors, assuming the field is constant. In addition, this paper reports several novel methods based on the new approach for batch and real time field sensors calibration. Finally, this paper reports a comparative evaluation of the proposed methods with numerical simulation and also reports comparative experimental evaluations with sensors onboard an underwater robot vehicle in the field. We note that unlike most previous studies of field sensor bias estimation, the present study reports a comprehensive comparison of the performance of the proposed novel approaches to the performance of several previously reported approaches. Parts of this study were preliminarily reported in [2]. The present paper includes several additional novel theoretical and experimental contributions that have not been previously reported. Among other contributions the concept of observability is included for each proposed method, a new comparative deep-sea field experimental evaluation, and a new section reporting an at-sea experimental evaluation as an application of the proposed methods for improved navigation of underwater vehicles.

This paper is organized as follows: Section I gives an introduction and overview of previously reported methods for field sensor calibration. Section II describes our general proposed approach for field sensor bias calibration and describes our proposed methods to solve for the measurement sensor bias. Section III describes the performance evaluation methodology used in this paper. Section IV reports a comparative numerical simulation results. Sections V and VI describe our laboratory and field experimental setup, respectively, and report comparative experimental evaluation of the performance of the different sensor bias estimation methods. Section VII describes, as illustration, a common application of the magnetometers for the case

G. Troni is with the Department of Mechanical and Metallurgical Engineering, Pontificia Universidad Católica de Chile, Santiago, Chile e-mail: gtroni@uc.cl and was previously with the Department of Mechanical Engineering, Johns Hopkins University, Baltimore, MD 21218, USA.

L. L. Whitcomb is with the Department of Mechanical Engineering, Johns Hopkins University, Baltimore, MD 21218, USA e-mail: llw@jhu.edu.

Digital Object Identifier 10.1109/TMECH.2019.2920367

1083-4435 © 2019 OAPA. Translations and content mining are permitted for academic research only.
Personal use is also permitted, but republication/redistribution requires IEEE permission.
See http://www.ieee.org/publications standards/publications/rights/index.html for more information.

of a dead reckoning underwater navigation and reports comparative experimental evaluation. Section VIII summarizes and concludes.

A. Related Work

Among the field sensor calibration the calibration of magnetometers has been studied extensively in the last decades. Several of these approaches have been or can be applied to the case of other 3D field sensors such as accelerometers. Several approaches for magnetometers calibration have been reported that estimate the calibration parameters without the use of additional references sensors. Traditional approaches include approximated solutions such as the conventional heading swing method, e.g., [3]. Recently, several reported methods have addressed more rigorously the three-axis magnetometer calibration problem. The problem of self-calibrating a three-axis magnetometer without external reference, can be formulated as an sphere or ellipsoid fitting problem. For estimating magnetometers bias, Gambhir proposed a "centered" approximation that can be solved with linear least squares [4]. This approach is inconsistent when using measurements corrupted by noise, [5], so different calibration approaches have been developed to overcome this problem. Alonso and Shuster proposed, the "TWOSTEP" method, that uses Gambhir's solution as initialization to an iterative second step for estimating the sensor bias [5] and, as reported in a later work, also estimates the scale and orthogonality factors [6]. In addition, Alonso and Shuster surveyed some of the previously reported magnetometer bias calibration methods [7]. Gebre-egziabher [8] proposed a linearized batch least squares method that is initialized using a nonlinear estimator. Vasconselos et al. [9] formulate the problem as an ellipsoid fitting problem, and solve it using an iterative maximum likelihood estimate (MLE) method. Similar methods have been considered to calibrate specifically the accelerometers based on the assumption that in static conditions the sensor is subjected only to gravitational force, e.g. [10], [11]. For practical implementation in different applications there are some limitations to these methods. In general, all of these calibration methods require large angular rotations of the instrument to measure a large section of the sensor output for an accurate calibration. For better performance it is necessary to know accurately the local magnitude of the Earth's magnetic or gravitational field. This value can be calculated by empirical models, e.g. [12], but can present large error in environments with unmodeled magnetic distortions (e.g., due to ferro-magnetic structures such as buildings or other local magnetic anomalies). Finally several of these methods are formulated for batch estimation and are not practical for continuous real time operation.

Although inertial sensors are commonly available with magnetometers in a combined instrument package, most previous reported methods for calibrating magnetometers do not utilize these additional sensors. Li and Li [13] and Kok et al. [14] make use of the accelerometers to measure the local gravity vector to propose methods to estimate the magnetometer calibration. The drawback of these approaches based on acceleration measurements is that translational accelerations of the instrument can perturb the measurements introducing errors in the magnetometer calibration.

Many applications require the ability to perform the field sensor calibration in real time due to (1) the calibration parameters changing during operations (e.g., due to change in vehicle payload) or (2) local field disturbances that render it impossible to estimate the calibration parameters before operation (e.g., for an underwater vehicle deployed from a large steel ship). Crassidis and Lai, [15], propose an extension to the TWOSTEP method based on the extended Kalman filter (EKF) and the unscented Kalman filter (UKF) to estimate in real time the sensor bias, scale, and orthogonality factors. Pylvanainen [16] proposed a recursive least squares method based on a linearized version of the ellipsoid fitting problem. Ma and Jiang proposed an alternative method based on the UKF, [17], and Guo at al., [18], reported an EKF approach. These methods exhibit some of the same problems noted for the batch methods, and also do not ensure convergence of the estimated parameters to the true values. Based on the same technique used by Alonso and others to compare the norm of the vectors in [19] the authors report an extension of the attitude estimator originally reported by [20] to estimates bias in the vector measurements. The drawback of this approach is the same as similar solutions based on the norm of the vector requiring large angular movements and to accurate know the local magnitude of the field. In some cases, such as indoor spaces, magnetometers measure a field with a non constant direction [21]. This is a different problem, however; it is not the focus of the present paper.

Based external-measurement sensors, such as cameras or range measurements, several methods have been proposed to estimate the accelerometer bias. Among them a very active community is related with visual-inertial methods (e.g., [22], [23]) where the gyroscope and accelerometer biases are continuously estimated. For magnetic sensor bias estimation, [24] proposed an ad hoc method, based on external measurements from a global navigation satellite system (GNSS) based two-antenna heading system. Troni and Eustice [25] reported an approach utilizing relative angular position measurements calculated—e.g., from multi-view image registration—to estimate the three-axis magnetometer measurement bias both as a batch process and also in real time. The drawback of these approaches are (i) they require additional sensors, (ii) they require external measurements that may be unavailable in many robotics applications, and (iii) if the relative angular position signal, from cameras or other sensors, is not available, they may be computationally intensive.

These previously reported approaches all share several limitations that limit their wide implementation: First, they require large angular movements. Second, they require accurate knowledge of the magnitude of the local field. Third, they are only available as batch methods or do not ensure convergence properties. The current paper reports a novel approach to the problem of accurate real time adaptive estimation of the sensor bias in three-dimensional field sensors. This approach employs three-axis angular velocity measurements from an angular-rate gyroscope to estimate the field sensor bias of a three-axis magnetometer or three-axis accelerometer (assuming the static case or compensated for linear accelerations). Three specific methods are proposed based on this novel general approach: one based on linear least squares, one Kalman filter approach, and one novel adaptive identification approach. Our main motivation is for the problem of magnetometers sensor bias, but it can also apply to other field sensors such as three-axis accelerometers. Recent results report simulation studies of bias estimation for both accelerometers and gyroscopes [26], but this falls beyond the scope of the present paper, and it does not change the general results of the present experimental evaluation. The novel proposed solution does not, at present, estimate scale and orthogonality factors. The proposed approach, which to the best of our knowledge has not been previously reported, exhibits several advantages: (1) it does not require the large angular movements required by previously reported approaches, (2) it does not require local field information, such as the magnitude and/or world-frame direction of the local magnetic or gravitational field, (3) it is implementable in real-time, and (4) it has provable convergence properties.

II. Proposed Approach and Methods

This section reports a novel approach to estimate the sensor measurement bias error in 3-axis field sensors (e.g. magnetometers) based on the instrument- frame angular-rate measurements (e.g., from angular-rate gyroscopes).

A. Mathematical Background

Matrices are denoted by capital letters, vectors and scalars are denoted by lowercase letters, and the dimensions of all symbols is stated explicitly. We represent the rigid body attitude using the rotation matrix $R(t) \in SO(3)$ describing the rotation from the instrument frame V to the inertial (world) fixed frame W. Let $\omega = [\omega_x, \omega_y, \omega_z]^\top \in \mathbb{R}^3$ and define the usual skew-symmetric operator $[\omega]_\times : \mathbb{R}^3 \to \mathbb{R}^{3\times 3}$

$$[\omega]_\times = \begin{bmatrix} 0 & -\omega_z & \omega_y \\ \omega_z & 0 & -\omega_x \\ -\omega_y & \omega_x & 0 \end{bmatrix}. \tag{1}$$

B. Novel Proposed Approach

Three-axis magnetometers and accelerometers are widely used in navigation applications. Measurements from these sensors are subject to systematic errors due to measurement sensor bias, scale factor and (lack of) orthogonality. We consider the usual model for measurement sensor bias

$$x(t) = \bar{x}(t) + b \tag{2}$$

where $\bar{x}(t) \in \mathbb{R}^3$ is the true field value in the instrument reference frame, $x(t) \in \mathbb{R}^3$ is the measured field value in the instrument reference frame, and $b \in \mathbb{R}^3$ is an unknown constant sensor bias.

Multi-axis field sensors such as magnetometers and accelerometers measure, in instrument coordinates, the Earth's local magnetic field—in the absence of local disturbances—or gravity vector field, respectively, which are each considered to be *locally* (∼hundreds of kms) constant and fixed with respect to the inertial world frame of reference. The true fixed world-frame field vector x_0 is related to the instrument-frame sensor measurement of the field $\bar{x}(t)$ by

$$x_0 = R(t)\,(x(t) - b). \tag{3}$$

In the case that the attitude of the instrument, $R(t)$, and the true field vector, x_0, are both known accurately, then solving for the unknown sensor bias, b, is trivial.

In many practical cases, however, such as the case of the ubiquitous micro-electro-mechanical systems (MEMS) inertial measurement units (IMUs) that are widely used in vehicle navigation systems, $R(t)$ *is not directly instrumented*—thus the trivial calibration solution is not applicable for these devices. MEMS IMUs are typically equipped with a 3-axis magnetometer, a 3-axis accelerometer, a 3-axis angular-rate gyroscope, and a temperature sensor.

Differentiating (3), yields

$$0 = \dot{R}(t)\,(x(t) - b) + R(t)\,\dot{x}(t). \tag{4}$$

Note that $\dot{x}_0 \approx 0$ is an approximation assuming the field is locally constant in the inertial reference frame. Using the standard equation $\dot{R}(t) = R(t)[\omega(t)]_\times$, we have

$$\dot{x}(t) = -\omega(t) \times (x(t) - b), \tag{5}$$

where $w(t)$ is the measured angular-rate in instrument coordinates, and $\times$ is the standard cross product operator. Note that the instrument attitude, $R(t)$, does not appear in (5).

This is the main contribution of the paper. Here we have reformulated a classic field sensors bias calibration problem in terms of the change of orientation, allowing for direct use of the angular-rate gyroscopes. In the next section we report three methods for bias-compensation based upon the novel proposed approach.

C. Proposed Methods Based on the Novel Proposed Approach

We wish to estimate the constant unknown sensor bias, b, for the system (5) from the signals $\omega(t)$ and $x(t)$. The proposed solutions include (*i*) a batch least squares method, (*ii*) a real time Kalman filter method, and (*iii*) a novel real time adaptive identification method.

1) Linear Least Squares for Sensor Bias Calibration: The unknown sensor bias, b, can be estimated with linear least squares estimation. The sum of squared residuals (SSR) cost function is

$$SSR(b) = \sum_{i=1}^{n} \frac{1}{\sigma_i^2} ||\dot{x}_i + \omega_i \times (x_i - b)||^2, \tag{6}$$

where σ_i is variance of the measurement, and each measurement x_i is a discrete sample measurement (e.g., x_i represents a discrete-time sampling of $x(t)$). The linear least squares estimate for b is given by

$$\begin{aligned} \hat{b} &= \underset{b\in\mathbb{R}^3}{arg\,min}\, SSR(b) \\ &= (\sum_{i=1}^{n} \frac{1}{\sigma_i^2} W_i^2)^{-1} (\sum_{i=1}^{n} \frac{1}{\sigma_i^2} W_i\, y_i), \end{aligned} \tag{7}$$

where $W_i \in \mathbb{R}^{3\times 3}$ is the skew-symmetric matrix from the measurements ω_i, $W_i = [\omega_i]_\times$, and $y_i \in \mathbb{R}^3$ is the calculated vector from the measurements, $y_i = \dot{x}_i + \omega_i \times x_i$.

Remark (Numerical differentiation)**.** *A drawback of this approach is that it requires the signal $\dot{x}(t)$, which for magnetometers and accelerometers can only be obtained by noisy numerical differentiation of the sensor measurement $x(t)$.*

Remark (Existence of solutions)**.** *The solution (7) exists when the set of measured angular velocity vectors, $[\omega_1, \omega_2, \cdots \omega_n]$ are not all collinear, in consequence, $(\sum_{i=1}^{n} W_i^2)$ is full rank and is thus invertible.*

2) Kalman Filter for Sensor Bias Calibration: The system (5) can be rewritten as

$$\underbrace{\begin{bmatrix} \dot{x} \\ \dot{b} \end{bmatrix}}_{\dot{\Phi}} = \underbrace{\begin{bmatrix} -[\omega]_\times & [\omega]_\times \\ 0 & 0 \end{bmatrix}}_{A(t)} \underbrace{\begin{bmatrix} x \\ b \end{bmatrix}}_{\Phi}, \tag{8}$$

with the measurement model

$$z = \underbrace{[I \;\; 0]}_{H} \begin{bmatrix} x \\ b \end{bmatrix}, \tag{9}$$

we can define the following linear time-varying (LTV) system

$$\begin{aligned} \dot{\Phi}(t) &= A(t)\,\Phi(t) + \nu_1(t), \quad & \nu_1(t) &\sim \mathcal{N}(0, Q), \\ z &= H\Phi + \nu_2(t), & \nu_2(t) &\sim \mathcal{N}(0, R). \end{aligned} \tag{10}$$

After a discretization of the continuous-time system the sensor bias estimation can be solved with a standard discrete-time Kalman filter implementation [27]–[29] that does not require differentiation.

Remark (Observability)**.** *The sufficient conditions for observability of the LTV system (10) can be shown by a rank test (see e.g [30], Theorem 9.10), the* $\operatorname{rank}\Theta = 6$*, where*

$$\Theta = \begin{bmatrix} I & 0 \\ -[\omega]_\times & [\omega]_\times \\ [\omega]_\times^2 - [\dot{\omega}]_\times & -[\omega]_\times^2 + [\dot{\omega}]_\times \end{bmatrix}. \tag{11}$$

Note that for full column rank of the matrix Θ, the equation $\Theta\, v \neq 0$ should hold for all $v \neq 0$. If $v = [v_1\; v_2]^\top$ then it is required that $[\omega]_\times v_2 \neq 0$ or $[\dot{\omega}]_\times v_2 \neq 0$ for all $v_2 \neq 0$. That is equivalent to $[\dot{\omega}]_\times \omega \neq 0$. Assuming $\omega(t)$ is continuous differentiable, then the system (10) is observable on $[t_0, t_f]$ if for some $t_a \in [t_0, t_f]$,

$$\dot{\omega}(t_a) \times \omega(t_a) \neq 0. \tag{12}$$

An interpretation of (12) is that the axis of rotation needs to vary during the time interval to make the system observable.

3) Adaptive Identification for Sensor Bias Calibration: The unknown sensor bias, b, can be estimated on-line with a novel adaptive identification algorithm which, to the best of our knowledge, has not been previously reported. The possible advantages of this adaptive approach are that (i) it does not require numerical differentiation of the sensor measurement $x(t)$, (ii) it is less computationally expensive than the previously proposed method based on Kalman Filter, and (iii) it could be combined with other nonlinear observer methods.

Consider the following adaptive observer for the plant of the form (5)

$$\begin{aligned} \dot{\hat{x}}(t) &= -\omega(t) \times (\hat{x}(t) - \hat{b}(t)) - k_1\, \Delta x(t),\ \hat{x}(0) = \hat{x}_0 \\ \dot{\hat{b}}(t) &= k_2\, (\omega(t) \times \Delta x(t)) \qquad\qquad ,\ \hat{b}(0) = \hat{b}_0, \end{aligned} \tag{13}$$

where estimation errors are defined as

$$\Delta x(t) = \hat{x}(t) - x(t), \quad \Delta b(t) = \hat{b}(t) - b. \tag{14}$$

Given the measured angular-rate signal, $\omega(t)$, and biased 3-axis field sensor measurement, $x(t)$, our goal is to construct an estimate of $\hat{b}(t)$ of the unknown sensor bias parameter b such that: 1) all signals remain bounded, and 2) $\hat{b}(t)$ converge asymptotically to b, i.e. $\lim_{t\to\infty} \Delta b(t) = 0$.

We first review some results that will be required later.

Definition 1 (**Persistency of Excitation [31], [32]**). *A matrix function $\mathcal{W}$: $\mathbb{R}^+ \to \mathbb{R}^{m\times m}$ is persistently exciting (PE) if there exists $T, \alpha_1, \alpha_2 > 0$ such that for all $t \geq 0$:*

$$\alpha_1\, I_m \geq \int_t^{t+T} \mathcal{W}(\tau)\, \mathcal{W}^\top(\tau)\, \mathrm{d}\tau \geq \alpha_2\, I_m \tag{15}$$

where $I_m \in \mathbb{R}^{m\times m}$ is the identity matrix. $M \geq 0$ is a generalized inequality meaning M is a positive semidefinite matrix.

Lemma 1 (**Barbalat's Lemma [33]**). *Let $\phi : \mathbb{R} \to \mathbb{R}$ be a uniformly continuous function on $[0, \infty)$. Suppose that $\lim_{t\to\infty} \int_0^t \phi(\tau)\ \mathrm{d}\tau$ exists and is finite. Then, $\phi(t) \to 0$ as $t \to \infty$.*

Lemma 2 (**Besacon's Lemma [34]**). *Given a system of the following form:*

$$\begin{aligned} \dot{e}_1 &= g(t)e_2 + f_1(t);\ e_1 \in \mathbb{R}^p, \\ \dot{e}_2 &= f_2(t) \end{aligned} \tag{16}$$

such that

1) $\lim_{t\to\infty} ||e_1(t)|| = 0$; $\lim_{t\to\infty} ||f_1(t)|| = 0$; $\lim_{t\to\infty} ||f_2(t)|| = 0$;
2) $g(t)$, $\dot{g}(t)$ *are bounded, and* $g^T(t)$ *is persistently exciting;*

then $\lim_{t\to\infty} ||e_2(t)|| = 0$.

We assume the following:

Assumption 1. *We assume the signals $\omega(t)$, $\dot{\omega}(t)$, and $x(t)$ are bounded, thus there exist three positive constants $\bar{c}_1$, $\bar{c}_2$, and $\bar{c}_3$ such that $\forall t$: $|\omega(t)| \leq \bar{c}_1$, $|\dot{\omega}(t)| \leq \bar{c}_2$, and $|x(t)| \leq \bar{c}_3$.*

We can now state the main result for the adaptive identifier.

Theorem 1 (**Sensor Bias Observer**). *Consider the system (5) with time-varying $\omega(t)$ and $x(t)$. Let $(\hat{x}, \hat{b})$ denote the solution to (13) with $k_1, k_2 > 0$ positive gains, and $\omega(t)$ satisfying the Assumption 1, and is PE as defined in Definition 1. Then the equilibrium $(\Delta x, \Delta b) = (0, 0)$ of (13) is globally asymptotically stable.*

Proof. From (13) and the estimation errors definition (14), the error system is

$$\begin{aligned} \Delta\dot{x}(t) &= -\omega(t) \times (\Delta x(t) - \Delta b(t)) - k_1\, \Delta x(t) \\ \Delta\dot{b}(t) &= k_2\, (\omega(t) \times \Delta x(t)). \end{aligned} \tag{17}$$

Consider the Lyapunov candidate function

$$\mathcal{L} = \frac{1}{2}||\Delta x||^2 + \frac{1}{2\, k_2}||\Delta b||^2 \tag{18}$$

where $\mathcal{L}$ is a smooth, positive definite, and radially unbounded function by construction. Differentiating and recalling (17) yields

$$\begin{aligned} \tfrac{d}{dt}\mathcal{L} &= \Delta x^\top[-\omega \times (\Delta x - \Delta b) - k_1\, \Delta x] + \Delta b^\top(\omega \times \Delta x) \\ &= -k_1\, ||\Delta x||^2 \ \leq 0. \end{aligned} \tag{19}$$

The time derivative of this Lyapunov function is negative semi-definite, thus guaranteeing global stability of the system, but additional arguments are needed to show global asymptotic stability. Given that the Lyapunov function (18) is bounded below by 0 and, in consequence of (19) is bounded above by its initial value, $\mathcal{L}_{t_0}$, and since (18) is a radially unbounded function of $\Delta x(t)$ and $\Delta b(t)$, we can conclude that $\Delta x(t)$ and $\Delta b(t)$ are bounded. Note that $\omega(t)$ is bounded from Assumption 1. From (17) and the fact that all signals on the right hand side of (17) are bounded then $\Delta x(t)$ and $\Delta b(t)$ are continuous and, in addition, $\Delta\dot{x}(t)$ and $\Delta\dot{b}(t)$ are bounded, thus $\Delta x(t)$ and $\Delta b(t)$ are uniformly continuous. For any t, we have $\int_0^t ||\Delta x(\tau)||^2\, \mathrm{d}\tau \leq \frac{1}{k_1}\, \mathcal{L}_{t_0}$ then $\Delta x(t) \in L^2$. Thus from Barbalat's lemma, we can prove globally asymptotically stability for $\Delta x(t)$. If $\Delta x(t) \to 0$ then $\Delta\dot{b}(t) \to 0$ as $t \to \infty$, but we need some extra results to prove asymptotically stability of $\Delta b(t)$. Since by assumption $[\omega(t)]_\times$ is PE and satisfies Assumption 1, using (Lemma 2) we can conclude globally asymptotically stability for $\Delta b(t)$. □

Remark. *The requirement of $[\omega(t)]_\times$ is PE as defined in Definition 1 give us observability condition similar to (12). The PE condition is only satisfied when the axis of rotation, or $\omega(t)$ direction, change over time.*

Remark. *The proposed observer based on (13) is globally asymptotically stable, although the gains $k_1, k_2 > 0$ can be used to change the performance of the observer. The first gain, k_1, adjust the learning rate of the estimated field sensor signal, thus changing the amount of filtering of the measured field sensor signal. The second gain, k_2, adjust the learning rate of the estimated bias signal.*

III. Evaluation Methodology

We compared the performance of six methods for field sensor bias estimation. Three batch estimation methods were evaluated:

a. *Centering*: For comparison purposes, the sensor bias is estimated using the first step of the TWOSTEP method [5] that leads to a simple batch linear least squares solution.
b. *TWOSTEP*: For comparison purposes, the sensor bias is estimated using the full TWOSTEP method [5].
c. ***SAR-LS*** (Sensor-bias based on Angular Rate - Least Squares method): The sensor bias is estimated using the batch method proposed in section II-C1 based on angular-rate in the instrument-frame. The value of $\dot{x}$ is numerically calculated by a first-order numerical differentiation of x. Furthermore the measurements are low-pass filtered to reduce noise resulting from differentiation.

In addition, three real time methods were evaluated:

d. *AI-EKF* (Attitude Independent - Extended Kalman Filter): For comparison purposes, the sensor bias is estimated using the real-time attitude independent previously proposed method based on the EKF [15]. The method based on the magnitude equation estimate the sensor bias requiring linearization to apply a standard EKF method. Note that for an accurate comparison the implemented version of this method only estimates the sensor bias, and not the scale and orthogonality matrix.

e. ***SAR-KF*** (Sensor-bias based on Angular Rate - Kalman Filter method): The sensor bias is estimated using the Kalman filter method described in section II-C2 based on angular-rate in the instrument-frame.
f. ***SAR-AID*** (Sensor-bias based on Angular Rate - Adaptive Identification method): The sensor bias is estimated using the adaptive identification method proposed in section II-C3 based on angular-rate in the instrument-frame.

Evaluated methods names are marked in bold-italic font. Previously proposed methods names used for comparison are marked only in italic font.

For comparison purposes, between batch estimation and real-time estimation methods, the sensor measurement bias used for the real-time estimation methods (AI-EKF, SAR-KF and SAR-AID) consists of the average of the last 20% of the estimated sensor measurement bias. The TWOSTEP and AI-EKF methods require knowledge of the local magnetic field magnitude. In our evaluation we employed the standard US/UK World Magnetic Model [12], [35]. To isolate from the angular-rate gyroscope bias effects, we have removed in post-processing the average of the in-water angular-rate measurements. Alternatively, it is possible to use the compensated data, available from the specific MEMS IMU attitude sensor used, but it does not change the general results in our experimental evaluation. Earth's rotation rate, $15^\circ/h$, is well below the noise floor of MEMS angular rate sensors, and thus Earth rate is neglected in the present analysis and also is neglected in the cited previous studies.

IV. Numerical Simulation Evaluation

A Monte Carlo simulation evaluation was implemented with 100 iterations for each of two datasets. Each iteration is a new smooth random sequence of angular movements starting from new initial angular positions. The first dataset, SIM1, simulates the case of large angular movements of the instrument in all degrees of freedom, depicted in Figure 3(a). The second dataset, SIM2, simulates a constrained angular movement of the instrument, depicted in Figure 3(b). The duration of each experiment is 60 s and the simulated sensor data is generated at 100Hz.

We consider the usual noise model adding Gaussian noise to the measurements of the magnetometers ($\sigma_{mag} = 1\,mG$) and angular-rate gyroscopes ($\sigma_{gyro} = 5\,mrad/s$). These values were in the same range than the sensors used in the experimental evaluation, as shown in Figure 2. The true magnetic field vector is $x_0 = [200,\ -40,\ 480]^\top$ mG and the bias is $b = [20,\ 120,\ 90]^\top$ mG. For a more realistic evaluation, the magnitude of the magnetic field used for estimation with the TWOSTEP and AI-EKF methods was 1% greater than the value used in generating the simulated data. In practice the magnetic field magnitude can significantly differ from magnetic models available due to magnetic distortions such as ferro-magnetic structures or other local magnetic anomalies. We have empirically selected the gains to obtain the best performance for each method under these The covariance matrices used by the AI-EKF and SAR-KF methods are $Q = 0.1 I_{6\times 6}$ mG$^2/s^2$ and $R = I_{3\times 3}$ mG^2. These values were chosen in the range of the expected process and sensor noises. The gains used by the SAR-AID method are $k_1 = 1$, $k_2 = 1$ for the SIM1 and $k_1 = 1$, $k_2 = 100$ for SIM2. These estimator gains were chosen empirically for the range of the instrument angular-rate for each experiment. Figure 4 shows the estimation performance for each simulated experiment.

The simulation results show that for a complete range of movements, SIM1, the batch methods Centered and TWOSTEP methods show the best performance. Although the proposed methods also estimate the magnetometer bias with an error under 1 mG. The worse performance is shown by AI-EKF method with bias estimation errors over 5 mG. The AI-EKF method is affected by linearization errors and does not ensure convergence. For the second dataset with a limited range of movements, SIM2, the SAR-LS, SAR-KF and SAR-AID methods show the best performance, with bias estimation errors under 2-3 mG. The other methods (Centered, TWOSTEP and AI-EKF) show a bias estimation error over 10 mG. Note that the TWOSTEP and AI-EKF methods are very sensitive to errors in a priori, known value of the magnitude of the local magnetic field. For small movements experiments (such as SIM2), we notice that the sensor bias estimation error grows proportionally to the error in the magnitude of the magnetic field. In our simulation performance evaluation, an error in the magnitude used for estimation is introduced representing a 1% of the real magnitude. But for common applications, the difference between the local magnitude of the magnetic field and the predicted by the model can include order of magnitude higher errors (such as inside/near ferro-magnetic buildings or other unknown magnetic anomalies).

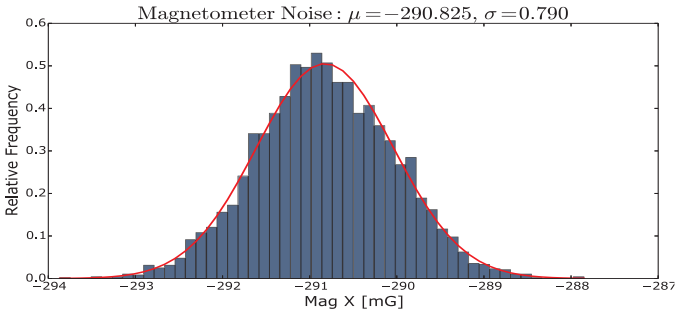

Fig. 2. Magnetometer Measurement Noise: Histogram showing the experimental sensor noise measured in a static setting.

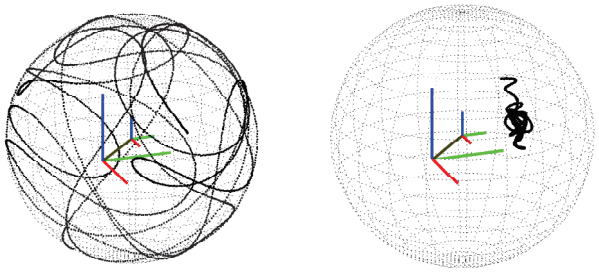

(a) Simulation Data SIM1 (b) Simulation Data SIM2

Fig. 3. Magnetometers simulated data: Three-dimensional plot of the magnetometers simulated data (black dots). The large reference-frame is at (0,0,0) with x-axis in red, y-axis in green, and z-axis in blue. The small reference-frame is at the center of the sphere at the known sensor bias b. The reference sphere depicted in the figure has a radius equal to the magnitude of the local magnetic field vector and centered at b.

It is interesting to notice that the required processing time on a Intel Core i7 computer for SAR-KF estimation was on average 13.1 s that is 5 times greater than the SAR-AID (2.5 s), and 6 times greater than the SAR-LS (2.2 s). This is due to the fact that the Kalman filter implementation is more computationally expensive than the implementation of the adaptive identification method or the batch least squares method.

The simulation results support the utility of all proposed methods. The next section reports a field experimental performance evaluation. The reader is directed to [2] for an additional laboratory experimental performance evaluation of these methods.

V. Laboratory Experimental Evaluation

This section reports the results of a comparative experimental performance evaluation of the six calibration methods in laboratory

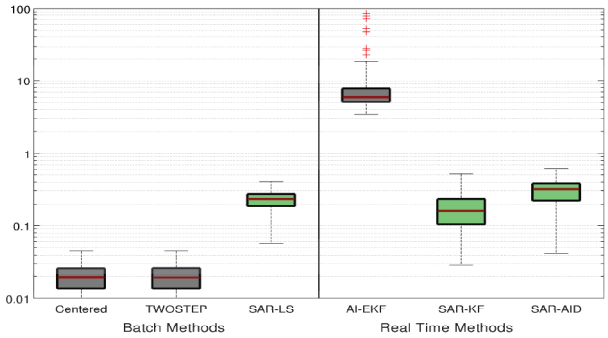

(a) Simulation results from SIM1

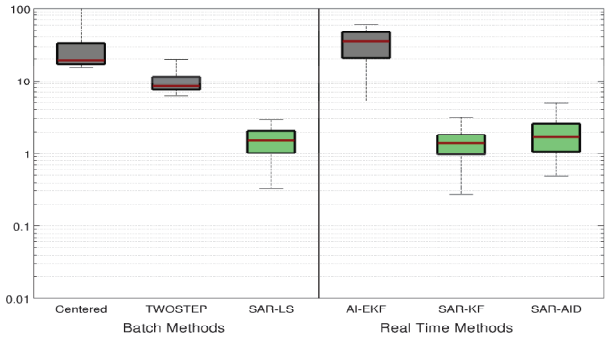

(b) Simulation results from SIM2

Fig. 4. Performance evaluation results from simulated data: The y-axis shows the sensor bias estimation error for each solution (mG) in logarithmic scale. Each box plot is calculated from 100 iterations.

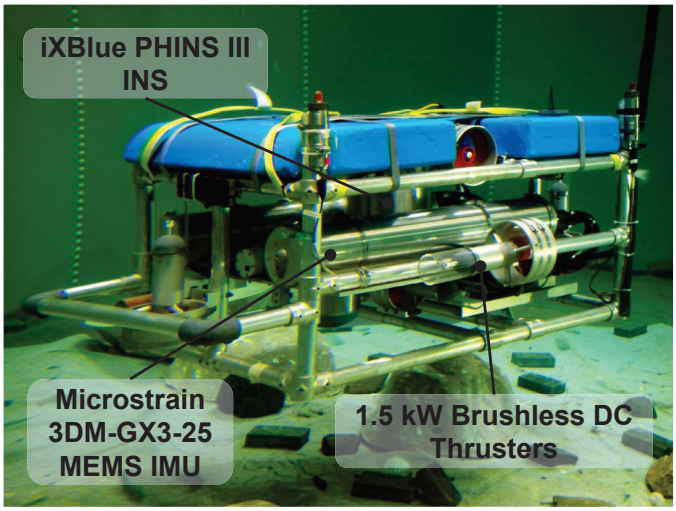

Fig. 5. JHU ROV submerged inside the Johns Hopkins Hydrodynamic Test Tank

experimental trials of an remotely operated underwater robotic vehicle (ROV) equipped with a MEMS IMU. The ROV is shown in Figure 5. The facility contains a 7.5 m diameter $\times$ 4 m deep indoor fresh water tank made of steel. The ROV is actuated by six 1.5 kW DC brushless electric thrusters and can be actively controlled in six degrees of freedom (DOF). A suite of sensors commonly employed in deep submergence underwater vehicles is present on the ROV. For our experimental performance evaluation we use a MEMS based IMU, the Microstrain 3DM-GX3-25 (LORD Sensing Systems, Williston, VT 05495, USA) [36]. The internal magnetometer's noise

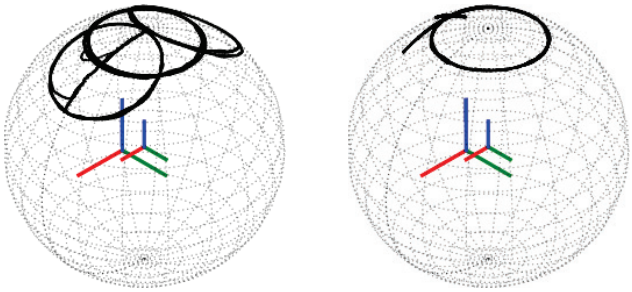

(a) Laboratory Data from EXP-L1 (b) Laboratory Data from EXP-L2

Fig. 6. Experimental evaluation laboratory data: Three-dimensional plot of the magnetometers recorded data for each experiment (black dots). The large reference-frame is at (0,0,0) with x-axis in red, y-axis in green, and z-axis in blue. The small reference-frame is at the center of the sphere at the SAR-AID estimated sensor bias b^*. The reference sphere depicted in the figure has a radius equal to the magnitude of the local magnetic field vector and centered at b^*.

level is $\sigma_{mag} = 1\,mG$ and angular-rate gyroscope's noise level is $\sigma_{gyro} = 5\,mrad/s$. Data was sampled and recorded at 100 Hz. For comparing the heading estimation performance, we used a high-end inertial navigation system (INS), the iXBlue PHINS III (iXBlue SAS, Saint-Germain en Laye, France) [37], as ground-truth. The PHINS provides heading with 0.05° accuracy, and pitch/roll with 0.01° accuracy. The high-end INS attitude data was re-sampled to the MEMS IMU sampling time to estimate the vehicle heading position.

Two experiments were performed. The first laboratory experiment, EXP-L1, measures a large range of movements, Figure 6(a). The trajectory is a sequence of 720° heading rotations, with three different levels of pitch (0° and $\pm$25°). These high-pitch dynamic trajectories are not feasible to implement in many ground, marine, or aerial vehicles. The second laboratory experiment, EXP-L2, measures a more feasible sequence of movements, Figure 6(b), where the range of movement of the vehicle is limited in pitch ($\pm$10°) and roll ($\pm$5°).

The magnetometers bias was estimated with each evaluated method using data from EXP-L1 and EXP-L2. From each estimated magnetometers bias, $\hat{b}_i$, we can calculate the heading error, between the heading from the magnetometers with the estimated bias $\hat{b}_i$ removed, hgd_i, and the heading from the high-end INS sensor, hdg_{REF}. First, for a self validation comparison, we use each experiment dataset to estimate the magnetometers bias and the same data to calculate the heading error. Second, for a cross validation comparison, we use each experimental dataset to estimate the sensor measurement bias, and then use each bias to correct the magnetometers measurements on a different experiment and calculate heading and heading error. The magnitude of the magnetic field used for the TWOSTEP and AI-EKF methods was 520 mG [35]. The covariance matrices used by the AI-EKF method are $Q_{AI-EKF} = 10 I_{33} mG$ and $R_{AI-EKF} = I_{33} mG$. The covariance matrices used by the SAR-KF method are $Q_{SAR-KF} = diag([4, 4, 4, 0.1, 0.1, 0.1])mG$ and $R_{SAR-KF} = I_{33} mG$. These values were chosen in the range of the expected process and sensor noises. The gains used by the SAR-AID method are $k_1 = 5$ and $k_2 = 100$. Table I and Figure 7 summarize the experimental results.

From the self validation performance evaluation, the SAR-LS, SAR-KF, and SAR-AID methods show a good performance in both experiments, correcting the heading error from the original 20-27° range to less than 2-3°. The SAR-LS performance is slightly worse than SAR-AID—we believe that this is due to the noise introduced by the numerical differentiation of the sensor measurement

TABLE I
SUMMARY OF THE SENSOR BIAS ESTIMATION RESULTS FROM EXP-L1 AND EXP-L2. BEST TWO PERFORMANCES IN EACH RELEVANT COLUMN IS MARKED IN BOLD FONT.

EXP-L1 for Calibration

	$\hat{b}_x$ [mG]	$\hat{b}_y$ [mG]	$\hat{b}_z$ [mG]	Self $\sigma(hdg_E)$ [degrees]	Cross $\sigma(hdg_E)$ [degrees]
Raw	0.000	0.000	0.000	27.362	20.478
Centered [5]	21.945	123.870	85.770	**2.377**	**0.857**
TWOSTEP [5]	21.940	123.867	85.676	**2.378**	**0.857**
SAR-LS	21.054	130.364	94.193	3.340	1.338
AI-EKF [15]	17.819	122.404	15.342	5.227	2.916
SAR-KF	21.703	130.259	106.288	3.277	1.409
SAR-AID	21.265	130.364	93.475	3.349	1.339

EXP-L2 for Calibration

	$\hat{b}_x$ [mG]	$\hat{b}_y$ [mG]	$\hat{b}_z$ [mG]	Self $\sigma(hdg_E)$ [degrees]	Cross $\sigma(hdg_E)$ [degrees]
Raw	0.000	0.000	0.000	20.478	27.362
Centered [5]	18.242	136.132	79.734	2.049	4.719
TWOSTEP [5]	18.246	136.180	78.641	2.064	4.750
SAR-LS	19.884	131.012	98.597	1.421	3.430
AI-EKF [15]	18.740	137.848	18.084	3.362	7.107
SAR-KF	20.072	119.145	105.158	**1.013**	**1.922**
SAR-AID	21.543	119.455	105.742	**0.959**	**1.923**

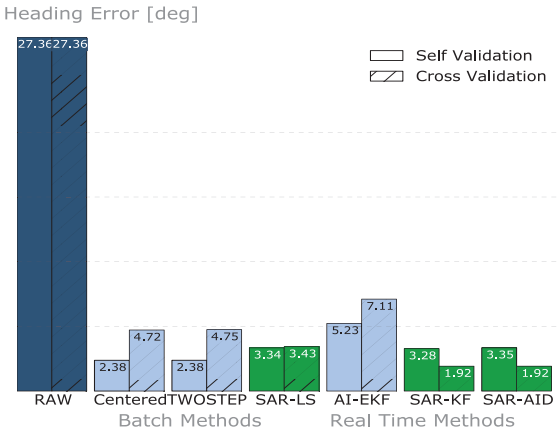

(a) Results EXP-L1

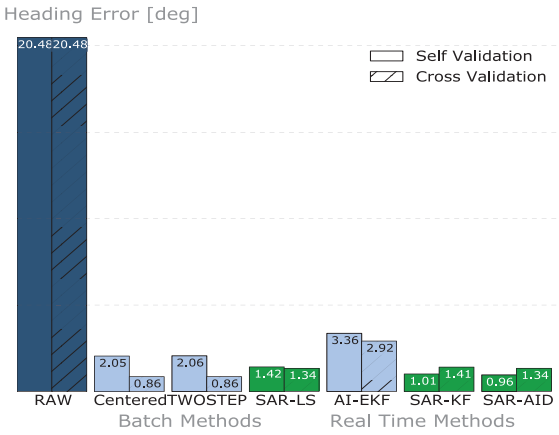

(b) Results EXP-L2

Fig. 7. Summary of the sensor bias estimation results from EXP-L1 and EXP-L2. The y-axis shows the heading error after calibration for each evaluated sensor bias estimation method. Self validation (solid): Heading error using the same data set for estimation and evaluation. Cross validation (dashed): Heading error using the other experiment for estimation and each for evaluation. All units in degrees.

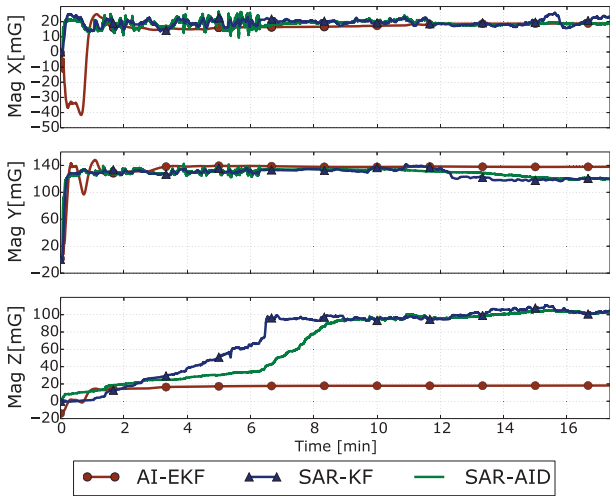

Fig. 8. Magnetometer bias estimation over time for EXP-L2: The x-axis shows the time (min) and the y-axis the estimated bias for each method (mG). In segmented red the AI-EKF method, in segmented dot blue the SAR-KF method, and in solid green the SAR-AID method.

required by the SAR-LS method. On the other hand, the Centered and TWOSTEP methods show a good performance for the first large angular movements experiment, but these methods have a less accurate performance for the more limited calibration dataset EXP-L2. For EXP-L2, the Centered and TWOSTEP methods show error that is twice of the error the proposed SAR-AID method. AI-EKF, like in the numerical simulations, shows the worse performance of the evaluated methods, although is still able to estimate the bias and improve the heading estimation, but not as good as the proposed methods (SAR-LS, SAR-KF, and SAR-AID).

From the cross performance evaluation, several interesting results were observed. When using EXP-L2—with a small range of movements—for calibration and EXP-L1—with a large range of movements—for evaluation, the SAR-LS, SAR-KF, and SAR-AID methods show a very good performance. Similar or even better performance than with self calibration with EXP-L1, showing been less sensitive to the range of movement. On the other hand, all the previously proposed methods (Centered, TWOSTEP, and AI-EKF) show a large increase of the error, showing that they are very sensitive to small range of movements. Finally, a less representative case, when using EXP-L1, with a large range of movements, for calibration and EXP-L2 for evaluation, all the methods are able to improve the performance compared to self calibration with EXP-L2. The exception is for the case of SAR-KF and SAR-AID that are able to obtain better performance with less range of movements. These methods are able to estimate online the measurement bias, so the fact that the experiments were performed in a steel test-tank with a non-uniform magnetic field affect their result when compared in a cross validation experiment. The next section show more representative cases in the case of field experiments.

Figure 8 shows the sensor bias estimation over time for the three

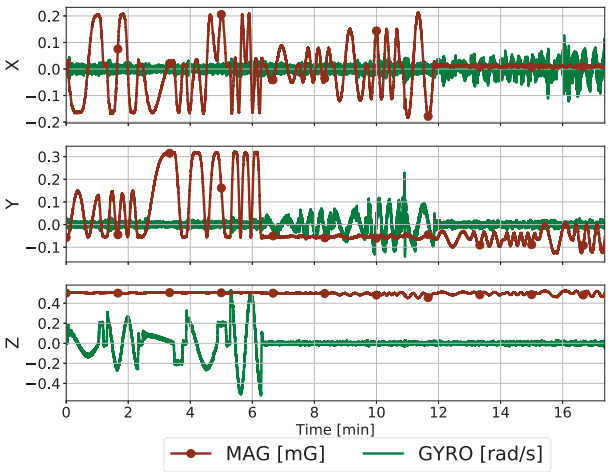

Fig. 9. Raw data over time for EXP-L2: The x-axis shows the time (min) and the y-axis the raw data for each sensor. In segmented red the magnetometer data [mG], and in solid green the angular-rate gyroscope data [rad/s].

Fig. 10. MBARI *R/V Western Flyer*, ROV *Doc Ricketts* and detail of the sensors used in the field experimental evaluation

real time evaluated methods (AI-EKF, SAR-KF, and SAR-AID) for EXP-L2. As a reference, Figure 9 shows the raw magnetometer and angular-rate gyroscope data for EXP-L2. The results show that all the methods converge quickly in b_x and b_y due to the nature of the excitation with large heading movements. But the term b_z, is correctly estimated, after limited movements in pitch and roll are applied, only for SAR-EKF and SAR- AID, but not for AI-EKF.

VI. Field Experimental Evaluation

This section reports the results of a comparative experimental performance evaluation of the six calibration methods in field experimental trials of a remotely operated underwater robotic vehicle (ROV) equipped with a MEMS IMU. The navigation data were obtained during oceanographic survey missions of the *Doc Ricketts* ROV operated from the *R/V Western Flyer*, Figure 10, conducted

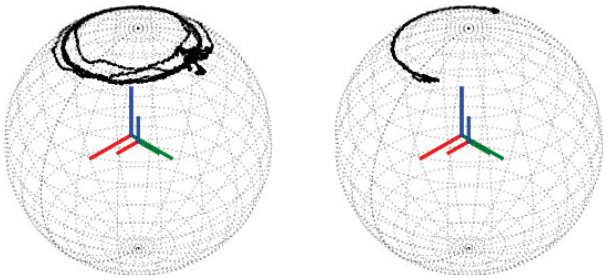

(a) Field Data from EXP-F1 (b) Field Data from EXP-F2

Fig. 11. Experimental evaluation field data: Three-dimensional plot of the magnetometers recorded data for each experiment (black dots). The large reference-frame is at (0,0,0) with x-axis in red, y-axis in green, and z-axis in blue. The small reference-frame is at the center of the sphere at the SAR-AID estimated sensor bias b^*. The reference sphere depicted in the figure has a radius equal to the magnitude of the local magnetic field vector and centered at b^*.

in December, 2014 in Monterey Bay at 2,800 m depth. The ship and ROV are owned and operated by the Monterey Bay Aquarium Research Institute (MBARI). *Doc Ricketts* ROV displaces 5,000 Kg, is rated to a depth of 4,000 meters.

For this experimental performance evaluation we use a MEMS based IMU, the Vectornav VN100 (VectorNav Technologies, LLC, Dallas, TX, USA) [38]. Its magnetometers' noise level is $\sigma_{mag} = 1\,mG$ and its angular-rate gyroscopes' noise level is $\sigma_{gyro} = 0.5\,mrad/s$. The MEMS IMU data was sampled and recorded at 80 Hz. For comparing the heading estimation performance, we used a high-end INS, the Kearfott Seadevil (Kearfott Corp., Little Falls, NJ, USA) [39], as 'ground-truth'. The Kearfott Seadevil includes a Doppler velocity log (DVL) as well as a ring-laser gyro and it provides heading with 0.05° accuracy, and pitch/roll with 0.03° accuracy. The real-time position estimation accuracy is 0.05% of the total distance traveled if the DVL continuously tracks the seafloor. The high-end INS data was sampled and recorded at 25 Hz. The MEMS IMU attitude data was interpolated to the high-end INS sampling time to estimate the vehicle heading position. Due to the lack of the precise knowledge of the real magnetometer bias, heading error is used as the used error metric for evaluation. To isolate from alignment errors, heading error is defined as the standard deviation between the measured heading from the high-end INS and the calculated heading from the bias compensated magnetometer data for each evaluated method. To isolate from the angular-rate gyroscope bias effects, we have removed in post-processing the average of the angular-rate measurements. Alternatively, it is possible to use the compensated data, available from the specific MEMS IMU attitude sensor used, but it does not change the general results in our experimental evaluation.

Two experiments were performed during the same day as part of a seafloor mapping survey dive. The first field experiment, EXP-F1, measures a sequence of movements, Figure 11(a). The trajectory is a sequence of 360° heading rotations, with changes on the vehicle configuration to produce (5°) pitch and roll movements. As a very common design the ROV is stable in pitch and roll due to a center of buoyancy and gravity separation, but with limited control on those axes. The second field experiment, EXP-F2, measures a 185 m long, "mowing the lawn", standard survey, Figure 11(b), where the range of movement of the vehicle is normally limited in pitch and roll.

The magnetometers bias was estimated with each evaluated method using data from EXP-F1 and EXP-F2. From each estimated magnetometers bias, $\hat{b}_i$, we can calculate the heading error, between the heading from the magnetometers with the estimated bias $\hat{b}_i$ removed, hgd_i, and the heading from the high-end INS sensor, hdg_{REF}. First,

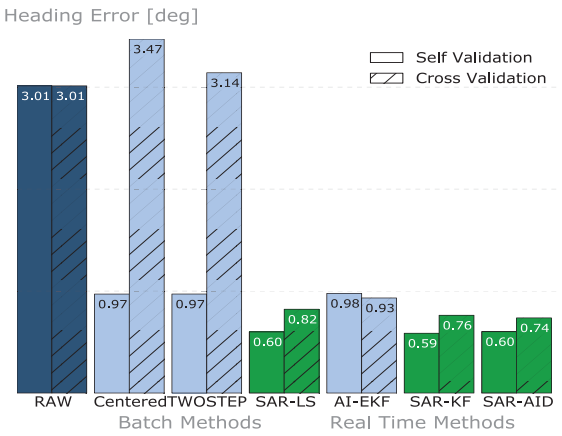

(a) Results EXP-F1 for evaluation

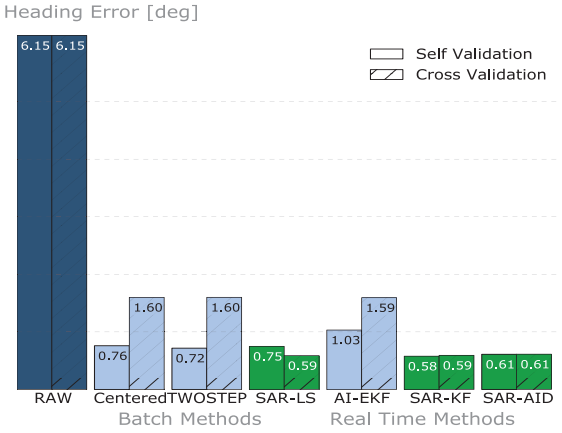

(b) Results EXP-F2 for evaluation

Fig. 12. Summary of the sensor bias estimation results from EXP-F1 and EXP-F2. The y-axis shows the heading error after calibration for each evaluated sensor bias estimation method. Self validation (solid): Heading performance using the same data set for estimation and evaluation. Cross validation (dashed): Heading performance using the other experiment for estimation. All units in degrees.

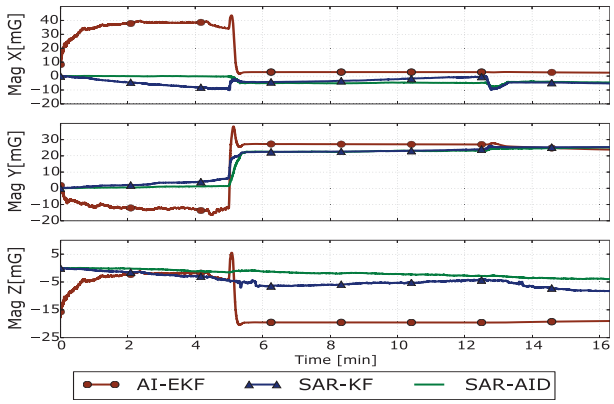

Fig. 13. Magnetometer bias estimation over time for EXP-F1: The x-axis shows the time (min) and the y-axis the estimated bias for each method (mG). In segmented red the AI-EKF method, in segmented dot blue the SAR-KF method, and in solid green the SAR-AID method.

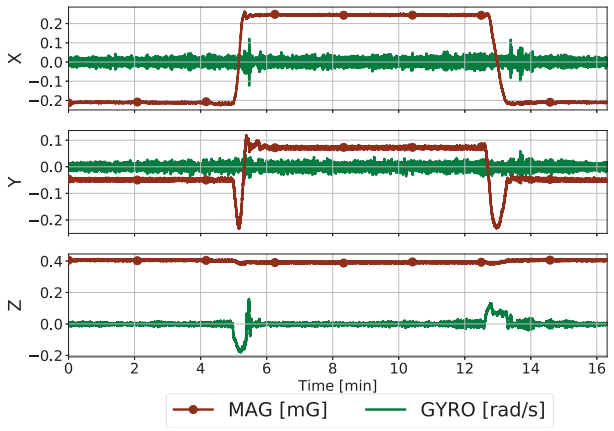

Fig. 14. Raw data over time for EXP-F2: The x-axis shows the time (min) and the y-axis the raw data for each sensor. In segmented red the magnetometer data [mG], and in solid green the angular-rate gyroscope data [rad/s].

for a self validation comparison, we use each experiment dataset to estimate the magnetometers bias and the same data to calculate the heading error. Second, for a cross validation comparison, we use each experimental dataset to estimate the sensor measurement bias, and then use each bias to correct the magnetometers measurements on a different experiment and calculate heading and heading error. The magnitude of the magnetic field used for the TWOSTEP and AI-EKF methods was 479 mG [35]. The covariance matrices used by the AI-EKF method are $Q_{AI-EKF} = 10I_{33}mG$ and $R_{AI-EKF} = I_{33}mG$. The covariance matrices used by the SAR-KF method are $Q_{SAR-KF} = diag([0.1, 0.1, 0.1, 0.001, 0.001, 0.001])mG$ and $R_{SAR-KF} = I_{33}mG$. These values were chosen in the range of the expected process and sensor noises. The gains used by the SAR-AID method are $k_1 = 2$ and $k_2 = 10$. Table II and Figure 12 summarize the experimental results.

For this particular case the required magnetometer calibration is minimal, less than 30 mG, a relatively small bias. This is an uncommon case but it highlights the importance of magnetometer calibration under even less critical cases. Under a small measurement bias the previously reported methods, specially AI- EKF, benefits from a reduction on the linearization errors and local minimum. Those limitation were shown in the simulation and experimental evaluation.

From the self and cross performance evaluation, the SAR-LS, SAR-KF, and SAR-AID methods show a very good performance in both experiments, with an excellent performance correcting the heading error from the original 3-6° range to less than 0.8°. On the other hand, the Centered, TWOSTEP and AI-EKF methods while show a good performance for the self calibration experiments, these methods have a less accurate performance for cross calibration evaluation. For all these previously reported methods the cross validation error increase between 55%-120% compared with the self validation error.

Figure 13 shows the sensor bias estimation over time for the three real time evaluated methods (AI-EKF, SAR-KF, and SAR-AID) for EXP-F2. As a reference, Figure 14 shows the raw magnetometer and angular-rate gyroscope data for EXP-F2. The results show that all the methods converge quickly in b_x and b_y due to the nature of the excitation with large heading movements. But the term b_z, is correctly estimated only for SAR-EKF and SAR-AID but not for AI-EKF. Even under a relative small bias and limited range of movement of the vehicle.

The numerical simulation and field experimental evaluation results all show an excellent performance of the proposed methods (SAR-LS, SAR-KF, and SAR-AID) for the case of heading estimation. But heading errors are due to several factors not only measurement bias error. In addition the results are averages over a full experiment and do not highlight the consistent bias in the measurement that can produce large errors on some applications such as navigation. On the

TABLE II
SUMMARY OF THE SENSOR BIAS ESTIMATION RESULTS FROM EXP-F1 AND EXP-F2. BEST TWO PERFORMANCES IN EACH RELEVANT COLUMN IS MARKED IN BOLD FONT.

EXP-F1 for Calibration						EXP-F2 for Calibration					
	$\hat{b}_x$ [mG]	$\hat{b}_y$ [mG]	$\hat{b}_z$ [mG]	Self $\sigma(hdg_E)$ [degrees]	Cross $\sigma(hdg_E)$ [degrees]		$\hat{b}_x$ [mG]	$\hat{b}_y$ [mG]	$\hat{b}_z$ [mG]	Self $\sigma(hdg_E)$ [degrees]	Cross $\sigma(hdg_E)$ [degrees]
Raw	0.000	0.000	0.000	3.012	6.148	Raw	0.000	0.000	0.000	6.148	3.012
Centered [5]	-1.856	33.194	-11.632	0.970	1.600	Centered [5]	11.281	15.599	266.008	0.760	3.471
TWOSTEP [5]	-1.861	33.209	-11.953	0.971	1.600	TWOSTEP [5]	10.097	16.884	237.761	0.717	3.140
SAR-LS	-3.044	26.958	-17.532	**0.600**	**0.589**	SAR-LS	-4.908	24.091	-16.312	0.749	0.822
AI-EKF [15]	-1.831	33.373	-16.106	0.977	1.594	AI-EKF [15]	2.672	24.826	-19.358	1.033	0.933
SAR-KF	-2.447	27.034	-16.415	**0.586**	**0.593**	SAR-KF	-4.939	25.358	-7.040	**0.578**	**0.763**
SAR-AID	-0.986	27.776	-20.778	0.644	0.618	SAR-AID	-2.578	27.298	-32.586	**0.602**	**0.657**

next section we show an application where the heading estimation is utilized in the position estimation of an underwater vehicle on a field experimental evaluation.

VII. APPLICATION TO UNDERWATER VEHICLE NAVIGATION

In underwater vehicle navigation the most common dead-reckoning navigation method is based on velocity measurements from the Doppler velocity log (DVL) combined with measurement from attitude and heading reference system (AHRS). In this case heading errors are a critical factor in position estimation [40].

This section reports the results of a comparative experimental performance evaluation of the six calibration methods in field experimental trials of an ROV equipped with a MEMS IMU and a DVL. These navigation data were obtained during a 135 minute survey mission of the *Doc Ricketts* ROV operated from the *R/V Western Flyer*, Figure 10, in Dec., 2014 in Monterey Bay at 2,800 m depth.

For magnetometer measurement bias calibration, we used the calibration parameters estimated on EXP-F1 and reported on Table II. The vehicle attitude, specially heading, is estimated with a nonlinear complementary filter, [41]. As a ground-truth position, we used the attitude and velocity measurements from the high-end INS, the Kearfott Seadevil [39], to estimate the vehicle position. Then we used the same velocities measurements but replace the attitude with the estimated attitude from each calibrated magnetometer data. Finally we can calculate the position error as the difference in between the estimated position and the 'ground-truth' position. Therefore the different position performance is due to the use of a different heading sources based on magnetometer measurements calibrated with each evaluated method. Figure 15 shows the norm of the XY position error corresponding to each magnetometer calibration method.

The position error for the case with magnetometer sensor without any calibration (RAW) is 138 m after 1,395 m of distance traveled. This represent around 10% of the distance traveled. The SAR-LS, SAR-KF, and SAR-AID methods show an excellent performance. All the proposed methods are able to calculate the position with an error less than 2 m. This represent around 0.2% of the distance traveled. On the other hand, the Centered, TWOSTEP and AI-EKF methods while are able to improve the performance after calibration, these methods have a less accurate position estimation performance with a position error around 2% of the distance traveled.

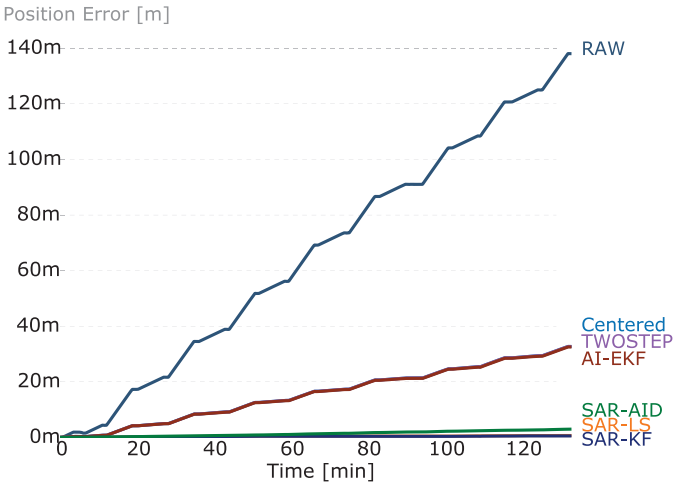

Fig. 15. Norm of the XY position error between the ground truth position from the Kearfott Seadevil INS and the calculated position based on heading estimated with the calibrated magnetometer measurements with each method.

VIII. CONCLUSIONS

The proposed angular-rate aided estimation methods (SAR-LS, SAR-KF, and SAR- AID) were shown to improve the sensor bias estimation performance under some circumstances compared with previously reported methods (Centered, TWOSETP, and AI-EKF).

A limitation shared with with all reported bias calibration methods is that they require angular motion of the instrument. And that an advantage of the approaches reported herein is that they do not require a-priori knowledge of the local magnetic field vector, and do not require knowledge of the instrument's real-time angular position, unlike previously reported methods which require one or both.

The numerical simulation, laboratory experimental results and field experimental results quantified the sensor measurement bias estimation performance under different scenarios of calibration motions. The proposed method, SAR-LS, SAR-KF and SAR-AID, show good performance for all the evaluated scenarios. Previously reported methods, Centered, TWOSTEP, and AI-EKF, show good performance only when the data represent large instrument angular motion. Moreover, TWOSTEP and AI-KF require exact knowledge of the magnitude of the local magnetic field.

The comparative laboratory and field experimental evaluation quantified the resulting calibrated heading estimation performance when compared with the heading reported by a high-end INS. The proposed method, SAR-LS, SAR-KF and SAR-AID, show significantly smaller heading error after calibration than all the previously reported methods for the case of a more feasible sequence of calibration movements for most ground, marine, or aerial vehicles. Furthermore the proposed methods (SAR-LS, SAR-KF, and SAR-AID) ensure convergence to the estimated sensor bias value while the real time method, AI-EKF,

does not ensure convergence to the true values. The simultaneously compensation for biases in both field sensors and angular-rate sensors is the subject our present research and will be addressed in future publications.

Finally as an application of the proposed methods for the case of a dead reckoning underwater vehicle navigation shows excellent results reducing the position estimation error from a 10% of the distance traveled to less than 0.2%. This compare favorably to previously reported methods that were able to only reduce the position error to around 2% of the distance traveled. These results should be useful to improve the performance of low-cost MEMS-based attitude sensors and, in consequence, improve the navigation accuracy for low-cost ground, marine, or aerial robotics vehicles.

ACKNOWLEDGMENT

This work was supported by the National Science Foundation under NSF award IIS-0812138. Support for the first author was also provided by CONICYT FONDECYT 11180907.

The field experimental data employed in this study were obtained during the 2014 Ocean Imaging cruise of the Monterey Bay Aquarium Research Institute (MBARI) aboard the *R/V Western Flyer* under the direction of Chief Scientist Dr. David Caress. We thank MBARI, and especially Dr. Caress, for the opportunity to collaborate on this sea trial. We gratefully acknowledge the contributions of H. Thomas, B. Hobson, and R. Henthorn for their contributions to the engineering development and to the *R/V Western Flyer* officers and crew.

REFERENCES

[1] J. Crassidis, F. Markley, and Y. Cheng, "Survey of nonlinear attitude estimation methods," *J. Guidance Control and Dynamics*, vol. 30, no. 1, p. 12, 2007.

[2] G. Troni and L. L. Whitcomb, "Adaptive estimation of measurement bias in three-dimensional field sensors with angular rate sensors: Theory and comparative experimental evaluation," in *Proc. Robot.: Sci. & Syst. Conf.*, (Berlin, Germany), June 2013.

[3] N. Bowditch, *American Practical Navigator*.

[4] B. Gambhir, "Determination of magnetometer biases using module RESIDG. Computer Sciences Corporation, Report No.3000-32700-01TN," tech. rep., Mar. 1975.

[5] R. Alonso and M. D. Shuster, "TWOSTEP, a fast robust algorithm for attitude-independent magnetometer bias determination," *J. Astronautical Sci.*, vol. 50, no. 4, pp. 433–451, 2002.

[6] R. Alonso and M. D. Shuster, "Complete linear attitude-independent magnetometer calibration," *J. Astronautical Sci.*, vol. 50, no. 4, pp. 477–490, 2002.

[7] R. Alonso and M. D. Shuster, "Attitude-independent magnetometer-bias determination: A survey," *J. Astronautical Sci.*, vol. 50, no. 4, pp. 453–476, 2002.

[8] D. Gebre-Egziabher, G. H. Elkaim, J. David Powell, and B. W. Parkinson, "Calibration of strapdown magnetometers in magnetic field domain," *Journal of Aerospace Engineering*, vol. 19, no. 2, pp. 87–102, 2006.

[9] J. F. Vasconcelos, G. Elkaim, C. Silvestre, P. Oliveira, and B. Cardeira, "Geometric approach to strapdown magnetometer calibration in sensor frame," *IEEE Trans. Aerosp. Electron. Syst.*, vol. 47, no. 2, pp. 1293–1306, 2011.

[10] I. Skog and P. Händel, "Calibration of a MEMS inertial measurement unit," in *XVII IMEKO World Congress, Brazil*, 2006.

[11] D. Tedaldi, A. Pretto, and E. Menegatti, "A robust and easy to implement method for IMU calibration without external equipments," in *2014 IEEE International Conference on Robotics and Automation (ICRA)*, pp. 3042–3049, May 2014.

[12] S. Maus, S. Macmillan, S. McLean, B. Hamilton, A. Thomson, M. Nair, and C. Rollins, "The US/UK World Magnetic Model for 2010-2015," tech. rep., Dec. 2010.

[13] X. Li and Z. Li, "A new calibration method for tri-axial field sensors in strap-down navigation systems," *Measurement Science and Technology*, vol. 23, no. 10, p. 105105, 2012.

[14] M. Kok and T. B. Schn, "Magnetometer calibration using inertial sensors," *IEEE Sensors Journal*, vol. 16, pp. 5679–5689, July 2016.

[15] J. L. Crassidis, K. L. Lai, and R. R. Harman, "Real-time attitude-independent three-axis magnetometer calibration," *J. Guidance Control and Dynamics*, vol. 28, no. 1, pp. 115–120, 2005.

[16] T. Pylvänäinen, "Automatic and adaptive calibration of 3D field sensors," *Applied Mathematical Modelling*, vol. 32, pp. 575–587, Apr. 2008.

[17] G.-F. Ma and X.-Y. Jiang, "Unscented Kalman filter for spacecraft attitude estimation and calibration using magnetometer measurements," in *Proc. Int. Conf. Machine Learning and Cybernetics*, (Guangzhou, China), pp. 506–511, Aug. 2005.

[18] P. Guo, H. Qiu, Y. Yang, and Z. Ren, "The soft iron and hard iron calibration method using extended Kalman filter for attitude and heading reference system," in *IEEE/ION Pos., Loc. and Nav. Symp.*, (Monterey, CA), pp. 1167–1174, May 2008.

[19] H. F. Grip, T. I. Fossen, T. A. Johansen, and A. Saberi, "Attitude estimation using biased gyro and vector measurements with time-varying reference vectors," *IEEE Trans. Automat. Contr.*, vol. 57, no. 5, pp. 1332–1338, 2012.

[20] R. Mahony, T. Hamel, and J.-M. Pflimlin, "Nonlinear complementary filters on the special orthogonal group," *IEEE Trans. Automat. Contr.*, vol. 53, no. 5, pp. 1203–1218, 2008.

[21] H. Ren and P. Kazanzides, "Investigation of attitude tracking using an integrated inertial and magnetic navigation system for hand-held surgical instruments," *IEEE/ASME Transactions on Mechatronics*, vol. 17, pp. 210–217, April 2012.

[22] M. Li and A. I. Mourikis, "High-precision, consistent EKF-based visual-inertial odometry," *The International Journal of Robotics Research*, vol. 32, no. 6, pp. 690–711, 2013.

[23] G. Panahandeh and M. Jansson, "Vision-aided inertial navigation based on ground plane feature detection," *IEEE/ASME Transactions on Mechatronics*, vol. 19, pp. 1206–1215, Aug 2014.

[24] J. Roth, C. Kaschwich, and G. Trommer, "Improving GNSS attitude determination using inertial and magnetic field sensors," *Inside GNSS*, vol. 7, no. 1, pp. 54–62, 2012.

[25] G. Troni and R. M. Eustice, "Magnetometer bias calibration based on relative angular position: Theory and experimental comparative evaluation," in *IEEE/RSJ International Conference on Intelligent Robots and Systems*, (Chicago, IL, USA), pp. 444–450, Sept. 2014.

[26] A. R. Spielvogel and L. L. Whitcomb, "Adaptive estimation of measurement bias in six degree of freedom inertial measurement units: Theory and preliminary simulation evaluation," in *Intelligent Robots and Systems (IROS), 2017 IEEE/RSJ International Conference on*, pp. 5880–5885, IEEE, 2017.

[27] R. Kalman, "A new approach to linear filtering and prediction problems," *J. Basic Engineering*, vol. 82, no. 1, pp. 35–45, 1960.

[28] Y. Bar-Shalom, T. Kirubarajan, and X.-R. Li, *Estimation with Applications to Tracking and Navigation*. 2001.

[29] S. Thrun, W. Burgard, and D. Fox, *Probabilistic Robotics*. MIT Press, 2005.

[30] W. Rugh, *Linear Systems Theory*. Prentice Hall, 2nd ed., 1996.

[31] S. Sastry and M. Bodson, *Adaptive Control: Stability, Convergence, and Robustness*. Prentice Hall, 1989.

[32] K. S. Narendra and A. M. Annaswamy, *Stable Adaptive Systems*. Dover, 2005.

[33] H. Khalil, *Nonlinear Systems*. Prentice Hall, 2002.

[34] G. Besancon, "Remarks on nonlinear adaptive observer design," *Systems and Control Letters*, vol. 41, no. 4, pp. 271 – 280, 2000.

[35] "The World Magnetic Model. National Oceanic and Atmospheric Admin. (NOAA).." http://www.ngdc.noaa.gov/geomag/WMM/DoDWMM.shtml.

[36] Microstrain Inc., *3DM-GX3-25 Miniature Attitude Heading Reference System datasheet.* Williston, VT, 2012.

[37] IXSEA, *PHINS III User Guide*. IXSEA, MU-PHINSIII-002 A ed., July 2008.

[38] Vectornav, *VN100 User Manual.* Dallas, TX, 2014.

[39] Kearfott, *Kearfott SeaNav*. Kearfott, 2015.

[40] G. Troni and L. L. Whitcomb, "Experimental evaluation of a MEMS inertial measurements unit for Doppler navigation of underwater vehicles," in *OCEANS 2012*, (Virginia Beach, VA), Oct. 2012.

[41] M. D. Hua, K. Rudin, G. Ducard, T. Hamel, and R. Mahony, "Nonlinear attitude estimation with measurement decoupling and anti-windup gyro-bias compensation," in *18th IFAC World Congress, Milano, Italy*, pp. 2972–2978, 2011.

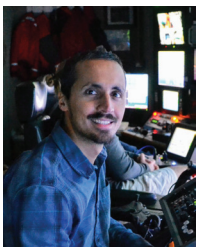

Giancarlo Troni (S'09–M'09) received the B.Sc. and M.Sc. degrees in electrical engineering from the Pontificia Universidad Católica de Chile (PUC), Santiago, Chile, in 1999 and 2001, respectively, and the Ph.D. degree in mechanical engineering from Johns Hopkins University, Baltimore, MD, in 2013. In addition, he was a Postdoctoral Research Fellow at the University of Michigan and the Monterey Bay Aquarium Research Institute working on underwater robotics.

Currently, he is an Assistant Professor with the Department of Mechanical Engineering, at the School of Engineering of PUC, Santiago, Chile. His research interests are in the areas of dynamics, mapping, estimation and control of field robotic systems, with a focus on marine vehicles.

Louis L. Whitcomb (S'87–M'87–SM'02–F'11) is Professor and former Chairperson (2013-2017) of the Department of Mechanical Engineering, with secondary appointment in Computer Science, at the Johns Hopkins Universitys Whiting School of Engineering. He is also an Adjunct Scientist, Department of Applied Ocean Physics and Engineering, Woods Hole Oceanographic Institution. He completed his Ph.D. in Electrical Engineering at Yale University. His research focuses on the navigation, dynamics, and control of robot systems, with applications to robotics in extreme environments including space and underwater robots. Whitcomb is a co-principal investigator of the *Nereus* and *Nereid Under-Ice (NUI)* Hybrid AUV/ROV Projects. He is the founding Director (2007-2013) of the JHU Laboratory for Computational Sensing and Robotics, the center of robotics research at JHU. He has received numerous best paper awards, teaching awards at Johns Hopkins University in 2001, 2002, 2004, and 2011, was the NSF Career Award, and the ONR Young Investigator Award. He is a Fellow of the IEEE.